Generating doughnut-shaped beams with large charge numbers by use of liquid-crystal spiral phase plates

Q. Wang, X. W. Sun, and P. Shum

Liquid-crystal spiral phase plates with cell gaps of 7 and 20 μm have been used to generate doughnut-shaped beams (doughnut beams) with charges of 1 and 4, respectively. Stacking these liquid-crystal spiral phase plates yielded doughnut beams with charge numbers up to 8. High efficiency and flexibility are the advantages of generating doughnut beams by stacking liquid-crystal spiral phase plates. Interference of doughnut beams generated by liquid-crystal spiral phase plates and plane waves has been studied. Fingerlike interference patterns were obtained with a doughnut beam tilted from a Gaussian beam; spiral fanlike patterns were obtained with a doughnut beam and a Gaussian beam collimated coaxially. The experimental results are supported qualitatively by simulation. By rotating a glass slide in the path of the Gaussian beam, one can rotate the fanlike interference pattern in a controlled fashion. With the liquid-crystal display technology that we have developed and report here, these liquid-crystal spiral phase plates should find applications in optical tweezers.

OCIS codes: 160.3710, 140.3300, 140.7010.

1. Introduction

A Laguerre–Gaussian (LG) beam is characterized by two indices for a given mode. A LG mode is generally represented by LG_p^l, where l is the azimuthal index that represents the number of 2π cycles in phase about the circumference and p is the radial index that represents $p + 1$ nodes along the radial direction. With radial index $p = 0$, LG modes appear in a doughnut-ring shape; they are usually called doughnut beams. Azimuthal index l in a LG beam often refers to a topographical charge for the doughnut beam. The doughnut beam has a helical wave front that is due to phase singularity. These helical wave fronts are known to give rise to an orbital angular momentum (OAM) that is $l\hbar$/photon for linearly polarized light.[1] The OAM is distinct from the angular momentum associated with the spin of a photon, which is known to be $\hbar$/photon. Obviously, a doughnut beam with a high topographical charge will lead to a large OAM. Great interest has been generated by the lure of potential applications of OAM. In particular, OAM can be used in optical tweezers,[2–4] which have been used in trapping and transferring angular momentum to microscopic particles or cells in biology applications. OAM has also found applications in guiding cooled atoms,[5] optical transformation,[6] frequency shifting,[7] and study of optical vortices.[8]

To generate a doughnut beam that carries OAM, three different classes of mode converters have been demonstrated: a cylindrical lens mode converter,[9] a hologram film,[10] and a spiral phase element.[11] Recently, there was a report of generating a doughnut beam by use of a liquid crystal (LC) spiral phase plate.[12] A LC spiral phase element has the advantages of high conversion efficiency and flexibility. As the fabrication of such a spiral phase plate is based on LC display technology that has already in existence, the cost is low. However, as the birefringence (Δn) of the LC is usually lower than 0.2, and the thickness (d) of the LC cell is usually less than 10 μm, the ability to change the LC retardation ($\Delta nd/\lambda$) is limited and hence the ability to generate a doughnut beam with a high topographic charge is limited. A doughnut beam generated with charge 2 and reported in Ref. 12 showed serious distortion.

The authors are with the School of Electrical and Electronic Engineering, Nanyang Technological University, Nanyang Avenue, Singapore 639798. X. W. Sun's e-mail address is exwsun@ntu.edu.sg.

Received 24 November 2003; revised manuscript received 15 January 2004; accepted 21 January 2004.

0003-6935/04/112292-06$15.00/0

However, a doughnut beam with a high topographic charge has advantages for applications in optical tweezers, as the OAM is proportional to the topographic charge (or to azimuthal index l). Using doughnut beams with higher azimuthal indices is more efficient in transferring energy from light to particles and cells being tweezed. In other words, a microscopic particle or cell to be tweezed can absorb less laser power if a higher-azimuthal-index doughnut beam is applied. This helps to reduce the rise in temperature that is due to absorption of light by the particle or cell. Thermal damage is quite common in biological applications; applying a doughnut beam with a high topographic charge will greatly alleviate thermal damage to cells.

To generate doughnut beams with high topographic charges we propose a scheme that entails stacking multiple LC spiral phase plates. The modulation of LC spiral phase plate stacks can be understood qualitatively as follows: When a plane laser beam with field U_0 passes through a $2\pi l$ spiral phase plate, the emerging ray becomes

$$U = U_0 \exp(il\theta), \tag{1}$$

where l is the number of 2π phase changes on any closed circle about the beam axis; it is the azimuthal index of the emerging doughnut beam. θ is the polar coordinate in the plane perpendicular to the beam propagation direction. In Eq. (1) the term $\exp(il\theta)$ is related to the $2\pi l$ spiral phase plate. Stacking n layers of LC spiral phase plates with $2\pi l_1$, $2\pi l_2$, . . . , $2\pi l_n$ spiral phase changes yields for the emerging ray

$$\begin{aligned} U &= U_0 \exp(il_1\theta)\exp(il_2\theta) \ldots \exp(il_n\theta) \\ &= U_0 \exp\left(i\theta \sum_i l_i\right), \end{aligned} \tag{2}$$

where i ranges from 1 to n. From Eq. (2) we can see that the azimuthal index of the emerging beam is the sum of all the azimuthal indices of the individual spiral phase plates. When Eqs. (1) and (2) are compared, the purity of the doughnut beam generated by the stacking method should be the same as that generated by a single spiral phase plate.

2. Structure and Stacking of Liquid-Crystal Spiral Phase Plates

A LC spiral phase plate was fabricated by a method similar to that reported in Ref. 12. Figure 1(a) is a photograph of the as-fabricated LC spiral phase plate with the rubbing direction and a scale bar indicated. Here we describe the structure and stacking of LC spiral phase plates. The LC cell consists of a LC layer sandwiched by two pieces of indium tin oxide (ITO) glass. The LC molecules are homogeneously aligned. The ITO electrode on one side of the LC spiral phase plate is lithographically patterned into a pie-shaped structure with 18 slices. Adjacent slices are separated by a 25-μm gap and are connected to etched ITO resistors of $\sim$600 Ω, except that two slices are connected to contact electrodes [Fig. 1(a)]. The

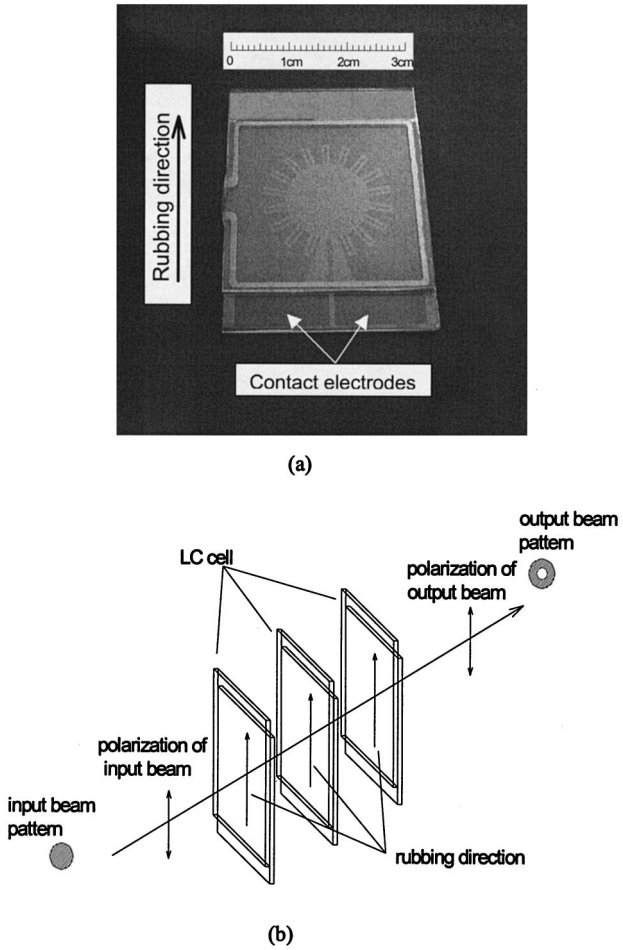

Fig. 1. (a) Photograph of a LC spiral phase plate with a scale bar and the rubbing direction indicated. The 18 slices and the ITO resistors can be seen clearly with slanted illumination. (b) Schematic showing the stacking of the LC spiral phase plates. The rubbing angles of the LC spiral phase plates should be parallel and the polarization of the input laser beam should be parallel to the rubbing direction as well.

counter-ITO electrode on the other side of the LC cell is not patterned; it is always grounded when the LC cell is in operation. It is worth mentioning that there is a circular area with a diameter of 140 μm in the center of the plate that cannot be modulated. LC cells with cell gaps of 7 and 20 μm were fabricated. A cell gap of 7 μm is widely used in commercial twisted nematic and supertwisted nematic displays. Stacking of LC spiral phase plates is done in such a way that the rubbing directions of all the stacked LC cells are parallel [Fig. 1(b)]. Ideally, the LC spiral phase plates should be glued with index-matched epoxy to reduce reflection loss; in our experiment they are simply loosely positioned together. Note that the polarization direction of the input laser beam should be parallel to the LC rubbing direction [Fig. 1(b)].

The birefringence of the LC mixture used in this experiment is 0.16. The retardation ($d\Delta n/\lambda$, where λ = 632.8 nm for the He–Ne laser used in our experiment) relative to the applied voltage of the LC cell as

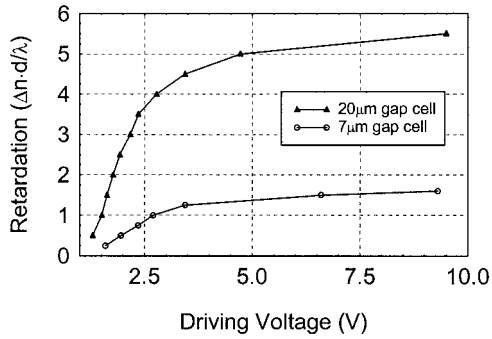

Fig. 2. Retardation ($\Delta nd/\lambda$) versus driving voltage for the fabricated LC spiral phase plates with cell thicknesses of 7 and 20 μm.

measured by an interferometer is shown in Fig. 2. In Fig. 2 the circles and triangles are measured data for LC spiral phase plates with cell gaps of 7 and 20 μm, respectively. It can been seen that, by applying a suitable driving voltage, one may obtain 2π and 10π phase shifts with 7- and 20-μm cells, respectively, for a He–Ne laser. And the retardation-voltage curves are quite linear to produce the above phase shifts.

When voltage is applied to the two contact electrodes [Fig. 1(a)], a linear voltage drop will be built up across the 18 slices by the series ITO resistors. The homogeneously aligned LC molecules respond to the voltage applied to each slice by tilting away from the glass (the LC molecules becomes more vertically aligned). The tilting angle, and hence the extraordinary refractive index seen by the incoming polarized beam [Fig. 1(b)], varies from slice to slice corresponding to the voltage drop across the cell. Accordingly, the extraordinary refractive-index variation in the helical direction will result in a helical phase delay across the 18 slices (Fig. 2).

3. Doughnut-Beam Generation

Images (a), (b), and (c) in Fig. 3 (top) show the far-field doughnut ring with, respectively, charges 1, 2, and 3

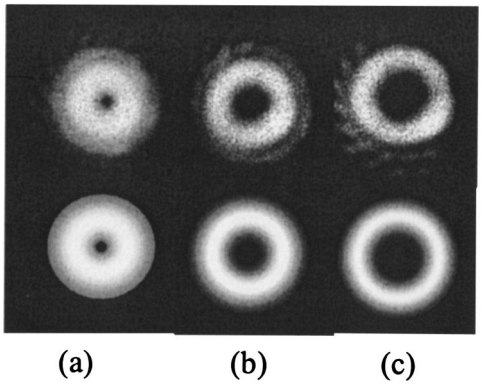

Fig. 3. Doughnut beams obtained in the experiment (top images) and the corresponding simulation results (bottom images): (a) with charge 1 generated with one 7-μm LC spiral phase plate, (b) with charge 2 generated by stacking of two 7-μm LC spiral phase plates, (c) with charge 3 generated by stacking of three 7-μm spiral phase plates.

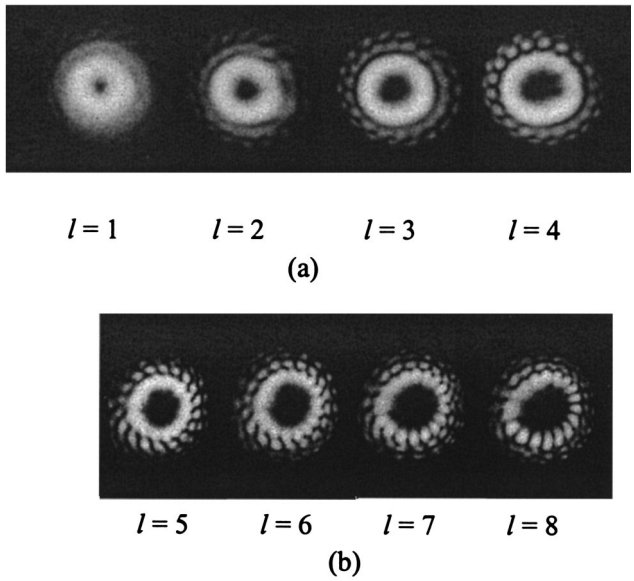

Fig. 4. Doughnut beams (a) with charges up to 4 (l = 1, 2, 3, 4) generated by one 20-μm-thick LC spiral phase plate and (b) with charges from 5 to 8 (l = 5, 6, 7, 8) generated by stacking of two 20-μm-thick LC spiral phase plates.

generated by one 7-μm LC cell and by stacking of two and three 7-μm LC cells. We obtained the images by placing the LC spiral phase plate or the stacks of plates at the output of a He–Ne laser. The bottom images in Fig. 3 show the corresponding results for doughnut beams with charges 1, 2, and 3 simulated by diffraction theory. The experimental results were in good agreement with the simulations. The charge number was determined from the retardation voltage curve shown in Fig. 2. It can be verified by comparison of the shape of the simulated doughnut beam with that of the experimental beam. It can be seen from Fig. 3 that, by stacking LC cells, one can obtain good-quality doughnut beams with large charge numbers. And it is rather easy to switch between doughnut beams with different charge numbers by adding or removing LC spiral phase plates. For example, we could obtain a charge-2 doughnut beam by stacking two LC spiral phase plates, each of which should generate a doughnut beam with charge 1 [Fig. 3(b)]. A doughnut beam with charge 3 could be obtained by stacking of three LC spiral phase plates, each of which should generate a doughnut beam with charge 1 [Fig. 3(c)]. It is worth mentioning that stacking two spiral phase plates with charges of 1 and -1 will cause the emerging ray to recover back to a Gaussian shape.

The LC spiral phase plates with the large, 20-μm cell gap were also characterized for generation of doughnut beams. Applying voltages to the 20-μm LC spiral plates yielded doughnut beams with charges 1 to 4, as shown in Fig. 4(a). The small-charge doughnut beams shown in Fig. 4(a) are of good quality. The slight distortion of the doughnut beam with charge 4 that can be observed from Fig. 4(a) comes from the nonlinear response of the retardation

Table 1. Gaussian-to-Doughnut Beam Conversion Efficiency of Single and Stacked LC Spiral Phase Plates[a]

Parameter	One 7-μm Plate	Two Stacked 7-μm Plates	Three Stacked 7-μm Plates	One 20-μm Plate	Two Stacked 20-μm Plates
Output power with no voltage applied (mW)	2.87	2.52	2.26	2.85	2.55
Output power with voltage applied (mW)	2.28[b]	1.70[c]	1.22[d]	2.27[e]	1.73[f]
Transparency (%)	89.7	78.8	70.6	89.1	79.7
Conversion efficiency (%)	79.4	67.5	54.2	79.6	67.8

[a]The total input power is 3.20 mW from a He–Ne laser operating at 632.8 nm. Transparency is the percentage ratio (output power without voltage applied/input laser power). The conversion efficiency is the percentage ratio (output power with voltage applied/output power without voltage applied). The voltages applied correspond to those shown in Figs. 3 and 4, respectively. The power is measured in the far field.
[b]Charge 1, Fig. 3(a).
[c]Charge 2, Fig. 3(b).
[d]Charge 3, Fig. 3(c).
[e]Charge 4, Fig. 4(a).
[f]Charge 5, Fig. 4(b).

versus applied voltage in the region just before the curve becomes flattened (Fig. 2). This region corresponds to the end of the transition from homogeous to homeotropic alignment of the LC molecules. Obviously, a larger optical retardation is needed for longer wavelengths. So a doughnut beam with large charge number and a longer wavelength tends to be more distorted than that with the same charge number and a shorter wavelength, as was also described in Ref. 12. However, this problem can be overcome by application of an individual voltage to each pie slice (not shown here). By stacking two 20-μm cells, we obtained doughnut beams with charges from 5 to 8 [Fig. 4(b)]. The outer rings in the surroundings of the doughnut beam (Fig. 4) are, in our opinion, due to diffraction in the gaps between adjacent slices and the unmodulated center of the input Gaussian beam (the center of the LC spiral phase plate is not modulated). These small coherent backgrounds combine with the singular beam, the splitting the vortex with a larger charge number.[13] To deter splitting, though it is impossible to avoid, the sizes of the unmodulated center and of the gaps between adjacent slices should be reduced. It can be seen from Fig. 4(b) that the doughnut with charge 8 becomes discrete (azimuthal modulation) and that the number of discrete elements equals the number of ITO slices. There are two possible causes of azimuthal modulation: (1) diffraction from the gap of adjacent slices and recombination of a (2) small coherent background with the singular beam, causing a vortex explosion in the resultant field, as has been reported to occur for a Bessel beam.[14] One can alleviate the azimuthal modulation by reducing the size of the gaps between adjacent slices and increasing the number of slices. The gaps between adjacent slices should be reduced to a level at which the LC molecules in the gap region can be strongly affected by potentials on two adjacent slices. According to research with liquid-crystal-on-silicon microdisplays,[15] a pixel-to-pixel gap of 1 μm (depending on the pretilt angle of the LC) is needed to eliminate the LC domain walls between the pixels. Thus we would expect a gap between adjacent slices to be reduced to at least 1 μm. For the two electrode slices of the LC spiral phase plate, because the voltages applied to them are so different, a smaller gap between them might be required.

4. Conversion Efficiency

A LC spiral phase plate has the advantage of nearly 100% conversion efficiency.[12] To verify this conclusion we measured the conversion efficiencies of single spiral phase plates and of stacked plates for our samples. The results are tabulated in Table 1. The input power is 3.2 mW from a 632.8-nm polarized He–Ne laser. Transparency is the percentage ratio (output power without voltage applied/input laser power). The conversion efficiency is the percentage ratio (output power with voltage applied/the output power without voltage applied). The power is measured in the far field. The voltages applied to the 7-μm cell and its two and three stacks are the same as those that we used to obtain doughnut beams in Fig. 3 and the voltages applied to the 20-μm cell and its two stacks are the same as were used to obtain the doughnut beams in Fig. 4, $l = 4$ and $l = 8$, respectively.

It can be seen from Table 1 that the transparencies of one 7-μm cell and one 20-μm cell are 89.7% and 89.1%, respectively. The loss of the static state (no voltage) is due mainly to the interface reflections between air–glass and glass–LC. The transparency of a single cell is not sensitive to the size of the LC cell gap. Neither is the conversion efficiency, which is 79.4% and 79.6% for one 7-μm cell and one 20-μm cell, respectively. Moreover, this conversion efficiency is independent of the charge number generated by a single LC plate. The dynamic loss (with voltage) comes from the diffraction of ITO electrode gaps. Stacking more LC spiral phase plates results in a slight, steady decrease in transparency and conversion efficiency. Stacking two 7-μm cells and three 7-μm cells reduces the transparency to 78.8% and 70.6%, respectively, and the conversion efficiency to 67.5% and 54.2%. Stacking two 20-μm cells to generate a doughnut beam with charge 8 yields the conversion efficiency of 67.8%, which is almost the

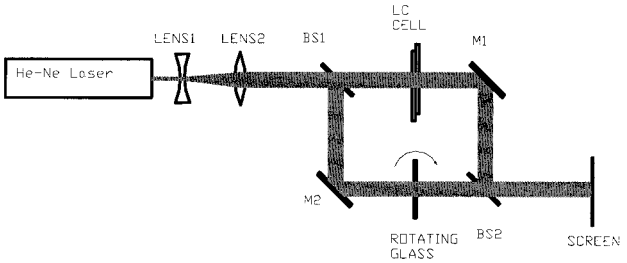

Fig. 5. Experimental apparatus with which to study the interference of a doughnut beam and a plane wave.

same as that achieved by stacking two 7-μm cells to generate a doughnut beam with charge 2. So the transparency and the conversion efficiency depend on the number of LC cells stacked but not on the charge number of the doughnut beam. Note that the reduction in transparency could be mitigated by use of index-matched epoxy to glue LC cells and antireflection coating at the air–glass interface, and the reduction in conversion efficiency could be decreased with small gaps between ITO slices. Only theoretically, 100% conversion efficiency is possible.

It should be noted that the actual conversion efficiencies are smaller than those tabulated in Table 1. This is so because the light that emerges from the LC spiral phase plate consists of LG beams with various radial indices p but the same azimuthal index l (assuming that the topological charge is conserved), including the doughnut beam with charge l ($p = 0$), which is the major component.[11] Moreover, because of the unmodulated center of the Gaussian beam (the center of the LC spiral phase plate is not modulated) and scattered and reflected light, there is a coherent background mixed with the singular beam that causes splitting of the vortex[13,14] (Figs. 3 and 4), resulting in larger charge numbers. The emerging ray should have more than one azimuthal index; i.e., the photon that emerges from the LC spiral phase plate possesses other values of OAM rather than $l\hbar$ only.

5. Vortex Generation

The interference between a doughnut beam and a plane wave was also studied. Figure 5 shows the experimental apparatus for generating the spiral interference pattern (vortex) of a doughnut beam and a plane wave. With a beam expander formed by two expanding lenses (LENS1 and LENS2), the diameter of the laser is expanded from 0.9 to 7 mm. A 50% beam splitter, BS1, is used to split the laser into two beams: One passes directly through the LC spiral phase plate and is then reflected by a M1 toward beam splitter BS2; the other beam is reflected by mirror M2 and passes through a glass slide and beam splitter BS2. The beam reflected by BS1 is recombined with the transmitted part at BS2. The LC spiral phase plate used is the 20-μm cell. The glass plate is used to vary the optical path of the plane wave to generate rotating interference patterns for

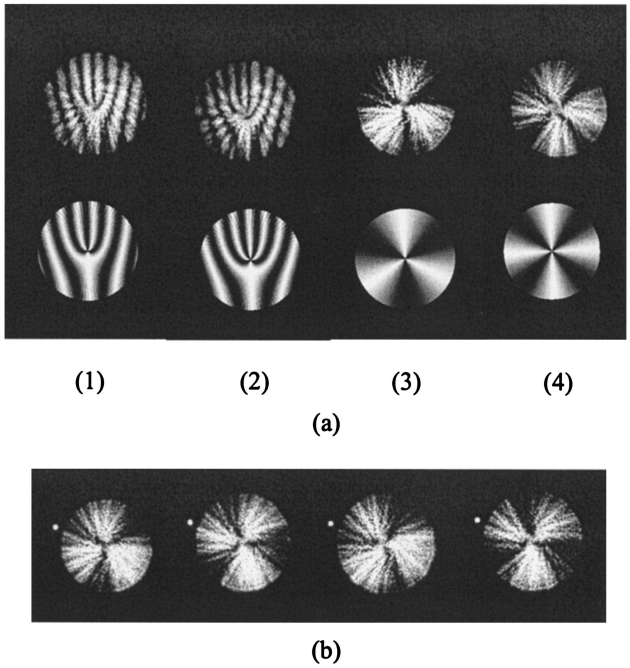

Fig. 6. (a) Interference patterns generated by doughnut beams of charges 3 (1) and 4 (2) with an inclined plane wave and 3 (3) and 4 (4) with a coaxial plane wave. The top images are experimental results, and the bottom images are simulations. (b) Rotating interference pattern generated by a doughnut beam of charge 3 and a coaxial plane wave. The bright dot at the left of each pattern was deliberately added as a reference to indicate the rotation.

particle and cell rotation. Interference patterns are observed in the near field.

Patterns 1 in Fig. 6(a) and 3 in Fig. 6(a) are interference patterns generated by a doughnut beam with charge 3 and an inclined plane wave and by a doughnut beam with charge 3 and a coaxial plane wave, respectively. Patterns 2 in Fig. 6(a) and 4 in Fig. 6(a) are interference patterns generated by a doughnut beam with charge 4 and an inclined plane wave and by a doughnut beam with charge 4 and a coaxial plane wave, respectively. The top images in Fig. 6(a) are the experimental results; the bottom images in Fig. 6(a) are the simulated results. The experimental results are in good agreement with the simulations. Through the interference pattern the charge number of the doughnut beam can also be determined. Here the doughnut beams generated are confirmed to carry charges of 3 and 4, respectively. By rotating the glass plate we observed rotation of the fanlike interference pattern. The recorded interference patterns are shown in Fig. 6(b). The four images shown in Fig. 6(b) correspond to four different orientations of the glass slide. The bright spot at the top left corner of each pattern in Fig. 6(b) provides a reference to show the rotation of the vortex. The rotating spiral interference pattern was applied to rotate optically trapped microscopic particles by use of a hologram,[4] but the power conversion efficiency was low. The response of the vortex to rotation is instantaneous with the rotation of the

glass slide. The response to changing the fan-out of the vortex (switching between different charge numbers of a doughnut beam) by varying the voltage applied to the LC spiral phase plate is in the range of tens of milliseconds, which is the typical range of a homogeous LC cell.

6. Conclusions

Liquid-crystal spiral phase plates with cell thicknesses of 7 and 20 μm have been fabricated. Doughnut beams with charges of 1 to 4 were generated by these LC spiral phase plates with cell thicknesses of 7 and 20 μm. We proposed stacking to obtain doughnut beams with large charge numbers. We obtained doughnut beams with higher charge numbers ($l = 8$) by stacking LC spiral phase plates. The advantages of stacking LC spiral phase plates to generate doughnut beams with large charge numbers are high conversion efficiency and flexibility. It is rather easy to switch between different charge numbers by adding or removing LC spiral phase plates. The spiral interference patterns were obtained by interference of a doughnut beam generated by a LC spiral phase plate and a plane wave. Interference patterns with doughnut beams tilted from Gaussian beams and the two beams collimated coaxially were obtained. The simulation results agreed qualitatively with the experimental interference pattern. By rotating a glass slide in the path of a Gaussian beam, we could rotate the fanlike interference pattern in a controlled fashion. With the LC display technology already developed, these LC spiral phase plates should find applications in optical tweezers and in any other situations in which a doughnut beam is needed.

References

1. L. Allen, M. W. Beijersbergen, R. J. C. Spreeuw, and J. P. Woerdman, "Orbital angular momentum of light and the transformation of Laguerre–Gaussian laser modes," Phys. Rev. A **45,** 8185–8189 (1992).
2. K. T. Gahagan and G. A. Swartzlander, Jr., "Optical vortex trapping of particles," Opt. Lett. **21,** 827–829 (1996).
3. N. B. Simpson, K. Dholakia, L. Allen, and M. J. Padgett, "Mechanical equivalence of spin and orbital angular momentum of light: an optical spanner," Opt. Lett. **22,** 52–54 (1997).
4. L. Paterson, M. P. MacDonald, J. Arlt, W. Sibbett, P. E. Bryant, and K. Dholakia, "Controlled rotation of optically trapped microscopic particles," Science **292,** 912–914 (2001).
5. X. Xu, K. Kim, W. Jhe, and N. Kwon, "Efficient optical guiding of trapped cold atoms by a hollow laser beam," Phys. Rev. A **63,** 340114 (2001).
6. S. N. Khonina, V. V. Kotlyar, M. V. Shinkaryev, V. A. Soifer, and G. V. Uspleniev, "The phase rotor filter," J. Mod. Opt. **39,** 1147–1154 (1992).
7. J. Courtial, D. A. Robertson, K. Dholakia, L. Allen, and M. J. Padgett, "Rotational frequency shift of a light beam," Phys. Rev. Lett. **81,** 4828–4830 (1998).
8. M. S. Soskin, V. N. Gorshkov, M. V. Vasnetsov, J. T. Malos, and N. R. Heckenberg, "Topological charge and angular momentum of light beams carrying optical vortices," Phys. Rev. A **56,** 4064–4075 (1997).
9. M. W. Beijersbergen, L. Allen, H. E. L. O. van der Veen, and J. P. Woerdman, "Astigmatic laser mode converters and transfer of orbital angular momentum," Opt. Commun. **96,** 123–132 (1993).
10. N. R. Heckenberg, R. G. Mcduff, C. P. Smith, and A. G. White, "Generation of optical phase singularities by computer-generated holograms," Opt. Lett. **17,** 221–223 (1992).
11. M. W. Beijersbergen, R. P. C. Coerwinkel, M. Kristensen, and J. P. Woerdman, "Helical-wavefront laser beams produced with a spiral phaseplate," Opt. Commun. **112,** 321–327 (1994).
12. K. Ganic, X. Gan, M. Gu, M. Hain, S. Somalingam, S. Stankovic, and T. Tschudi, "Generation of doughnut laser beams by use of a liquid-crystal cell with a conversion efficiency near 100%," Opt. Lett. **27,** 1351–1353 (2002).
13. M. S. Soskin, V. N. Gorshkov, M. V. Vasnetsov, J. T. Malos, and N. R. Heckenberg, "Topological charge and angular momentum of light beams carrying optical vortices," Phys. Rev. A **56,** 4064–4075 (1997).
14. S. Orlov, K. Regelskis, V. Smilgevicius, and A. Stabinis, "Propagation of Bessel beams carrying optical vortices," Opt. Commun. **209,** 155–165 (2002).
15. Y. L. Zhang, P. J. Bos, and D. B. Chung, "2-D modeling of the effect of electrode topography and interpixel gap on LCoS devices," in *Society for Information Display, International Symposium Digest of Technical Papers* (Society for Information Display, San Jose, Calif., 2003), Vol. XXXIV, pp. 1382–1385.